Generating structural distributions of atomistic models of Li_2O nanoparticles using simulated crystallisation†

Thi X. T. Sayle,[a] Phuti E. Ngoepe[b] and Dean C. Sayle*[a]

Received 24th May 2010, Accepted 16th July 2010
DOI: 10.1039/c0jm01580f

Simulated crystallisation has been used to predict that Li_2O nanoparticles comprise octahedral morphologies bounded by {111} and truncated by {100} with inverse fluorite crystal structure. We observe that by changing the temperature of the (simulated) crystallisation, changes in the microstructure can be realised, such a strategy facilitates the generation of full atomistic models with microstructural distributions similar to the structural diversity observed synthetically.

Introduction

Atomistic computer simulation has, for over 60 years,[1] been used to generate atomistic models for materials, which are then exploited to predict pertinent properties to inform experiment. However, many properties are influenced or indeed governed by the microstructure[2] and therefore if simulation is to be used to predict the properties with sufficient accuracy that they are of value to experiment, then such microstructure needs to be captured within the structural model. Microstructural features may include, for example, morphology, point defects, dislocations, and grain-boundaries. Moreover, the explosive growth in nanomaterials research[3] has led to particular microstructural features being promoted to higher significance. For example, for nanoparticles, there are higher concentrations of surface ions, compared to bulk ions, together with increased exposure of edges and corners;[4] for mesoporous materials, the implications of curved surfaces, both convex and concave, may prove pivotal to its properties.[5]

Many atomistic simulations use symmetry operators to generate the atomistic model,[6] which can be extended to include surfaces and interfaces.[7] Equipped with a pristine model, microstructural features such as point defects are now routinely introduced,[8,9] and while extended defects are more problematic, strategies are available to incorporate dislocations,[10,11] grain-boundaries (GB)[12] and heterointerfaces[13–15] within the atomistic model. However, a real material is likely to comprise several microstructural features—including their synergy of interaction. For example, a nanoparticle will comprise a variety of surfaces, steps, edges corners, point defects (vacancies, interstitials and dopants) and perhaps grain-boundaries and dislocations. Experiment shows that nanoparticles are rarely identical; rather a (size and shape) distribution necessarily derives from the synthetic method used in their manufacture.[16] To include all such features within a single atomistic model using, for example, symmetry operators, becomes more complex. On the other hand there has been a tremendous advance in experimental observation, where three-dimensional images are now available and can be used to help validate the theoretical model.[16,17]

Clearly, if the microstructural features evolve directly from the synthetic method, then arguably the best way to capture them is to (attempt to) 'simulate synthesis' dynamically. Indeed, there have been many studies that endeavour to achieve this goal, for example see ref. 18–20. However, a key weakness of simulating synthesis, using for example, molecular dynamics (MD) are the short timescales accessible to MD, but these limitations are being surmounted using simulation strategies such as temperature assisted dynamics[21] and Monte Carlo[22] methods—and especially using combinations of simulation strategies.[21] In addition, innovative strategies such as genetic algorithms[23] and neural networks[24,25] have also been used to explore microstructure.

Here, we use simulated crystallisation to generate an atomistic model of a nanostructure, which includes a variety of microstructural features. In particular, the material is first amorphised and then crystallised. Moreover, similar to experiment one cannot choose which structure evolves; rather the structure evolves 'naturally' as directed by the interatomic potential used to describe the material and in response to the simulation conditions imposed such as temperature and pressure.[26] Nevertheless it has been used successfully to generate atomistic models of nanostructured materials with crystal structures including: rock salt,[19] fluorite,[27] rutile[26] and α-PbO_2.[26] Here we extend this list to include an inverse fluorite structured material. Specifically, we use simulated crystallisation to generate models for Li_2O nanoparticles.

Lithium oxides are of interest in technologically important areas such as energy storage[28,29] and nuclear.[30,31] Recently, nanostructured (energy) materials have been exploited for their high surface area and short pathways for Li-ion transport with implications for fast charge and high current output[28] in rechargeable batteries. Moreover, the nanomaterial can sustain a high (elastic) expansion and contraction, associated with intercalation of the Li charge carriers, compared to structural collapse suffered by the parent bulk material.[32] The implications for ionic conduction are similarly intriguing.[33] Clearly, to determine the implications of traversing to the nanoscale with respect to structural and property changes, and the associated impact such factors have upon potential applications, efforts focussed upon nanostructured lithium oxide are needed.

[a]*DEAS, Cranfield University, Defence Academy of the United Kingdom, Shrivenham, SN6 8LA, UK. E-mail: d.sayle@cranfield.ac.uk*
[b]*Materials Modelling Centre, School of Physical and Mineral Sciences, University of Limpopo, Private Bag x1106, Sovenga, 0727, South Africa*
† This paper is part of a *Journal of Materials Chemistry* themed issue on Modelling of Materials. Guest editors: Julian Gale and Mark Wilson.

Method

In this section we outline the potential model used to describe Li_2O, the simulation code used to perform the molecular dynamical simulations and the strategy used to generate the atomistic models of Li_2O nanoparticles.

Potential model

All calculations, presented in this study, were based upon the Born model of the ionic solid, where the energy, E, of the system is given by:

$$E(r_{ij}) = \sum_{ij} \frac{Q_i Q_j}{4\pi\varepsilon_o r_{ij}} + \sum_{ij} A \exp\left(\frac{-r_{ij}}{\rho}\right) - C r_{ij}^{-6},$$

the first term represents the Coulombic interaction between ion i of charge Q_i and ion j of charge Q_j, which are a distance r_{ij} apart. The second term is of the Buckingham form, which is particularly effective in representing ionic solids. Model parameters, used to describe Li_2O, are presented in Table 1 and were taken from ref. 34.

Simulation code

The DL_POLY code was used to perform all the molecular dynamics (MD) simulations; the user manual provides comprehensive analytical descriptions and discussion of the molecular dynamics simulations, force fields, boundary conditions, algorithms and parallelisation methods used in these simulations. Further details are available in ref. 35.

Atomistic model generation

Three cubes of Li_2O, each comprising 17 576 Li^+ ions and 8788 O^{2-} ions, were cut from the parent (bulk) material and tensioned by 30%. Each cube was then amorphised, crystallised and cooled using constant volume molecular dynamics; simulation conditions are shown in Table 2. The time step was set to 0.001 ps for the amorphisation stage, and 0.005 ps for the crystallisation and cooling steps. We note that the amorphisation was sufficient to remove any crystallinity pertaining to the inverse fluorite structure; calculated radial distribution functions were broad, which is indicative of an amorphous rather than crystalline structure. This is to ensure that the starting structure does not influence, perhaps erroneously, the final structure of the nanoparticle, which is influenced solely by the interatomic potentials describing the Li_2O and the simulation conditions. Moreover, the crystalline seed must evolve spontaneously within the amorphous sea of ions and not templated from any residual inverse-fluorite structure already present within the system.

Table 1 Interionic potential parameters of the form $E(r_{ij}) = \sum_{ij} \frac{Q_i Q_j}{4\pi\varepsilon_o r_{ij}} + \sum_{ij} A \exp\left(\frac{-r_{ij}}{\rho}\right) - C r_{ij}^{-6}$ used to describe the Li_2O nanoparticles

Interaction	A/eV	ρ/Å	C/eV Å^6	Charge
O^{2-}–O^{2-}	11 782.8	0.234	30.22	−1.1
Li^+–O^{2-}	30 000.0	0.154	0.000	
Li^+–Li^+	270 000.0	0.143	0.000	0.55

Results

The configuration energies, calculated as a function of time, for each nanoparticle (A), (B) and (C) are shown in Fig. 1(a–c) respectively; the radial distribution function (RDF) for nanoparticle (A), calculated at various time intervals during the crystallisation, is shown in Fig. 1(d).

We first consider nanoparticle (A): at the start of the simulation, the energy is high (less stable), which is indicative of an amorphous configuration. The energy plateaus initially and then starts to fall. Analysis of the crystallisation (nanoparticle A) using molecular graphical techniques revealed that a crystalline seed conforming to the inverse fluorite crystal structure

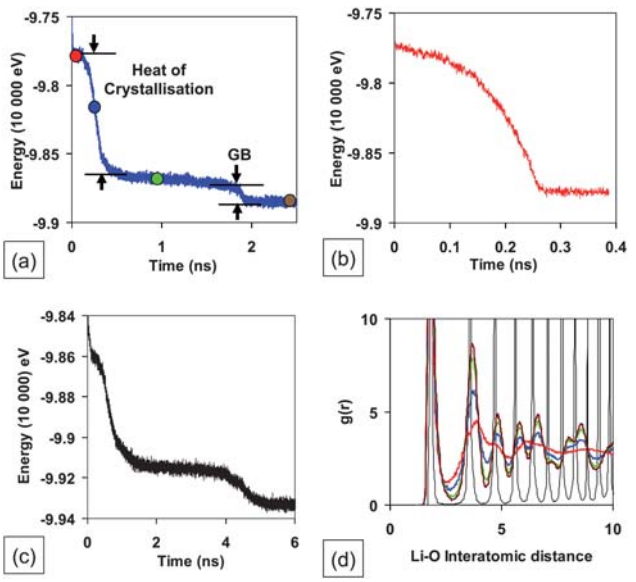

Fig. 1 Configuration energy calculated as a function of time during crystallisation. (a) Li_2O nanoparticle (A); (b) Li_2O nanoparticle (B); (c) Li_2O nanoparticle (C). (d) Radial distribution function (RDF) for Li_2O nanoparticle (A), calculated after: 130 ps (red), 260 ps (blue), 1000 ps (green), 2000 ps (brown) and for the final, 1 K structure (black). The RDF can be usefully correlated with (a), on which are shown coloured circles corresponding to the RDF.

Table 2 Simulation conditions used to generate the atomistic models for Li_2O nanoparticles

Nanoparticle	Amorphisation	Crystalisation	Cooling	Configurational energy
A	1000 K, 20 ps	800 K, 2.5 ns	1 K, 250 ps	102 691.3 eV
B	800 K, 50 ps	800 K, 385 ps	1 K, 250 ps	102 616.4 eV
C	1000 K, 20 ps	700 K, 19 ns	1 K, 250 ps	102 603.2 eV

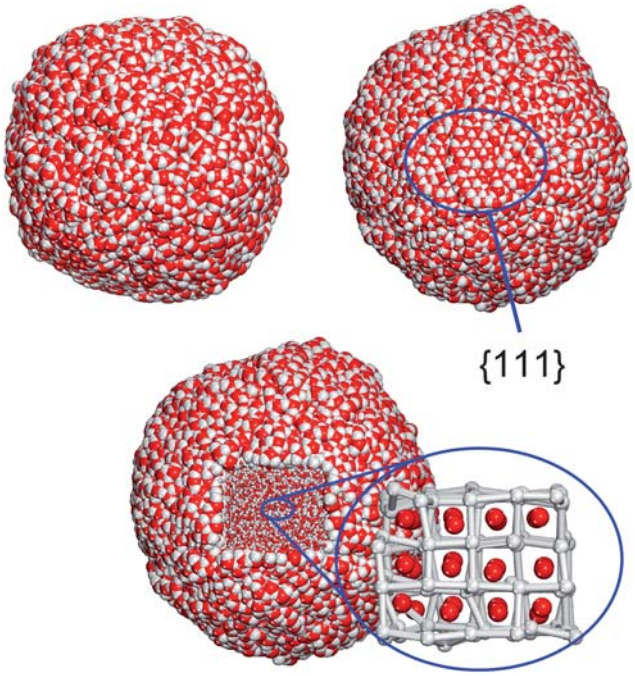

Fig. 2 Structure of the amorphous Li_2O nanocrystal (A) top left, and, top right, after a crystalline seed had spontaneously evolved (blue circle) at the surface. The lower figure reveals that the nucleating seed conforms to the inverse fluorite structure. Red spheres are oxygen and grey spheres are Li.

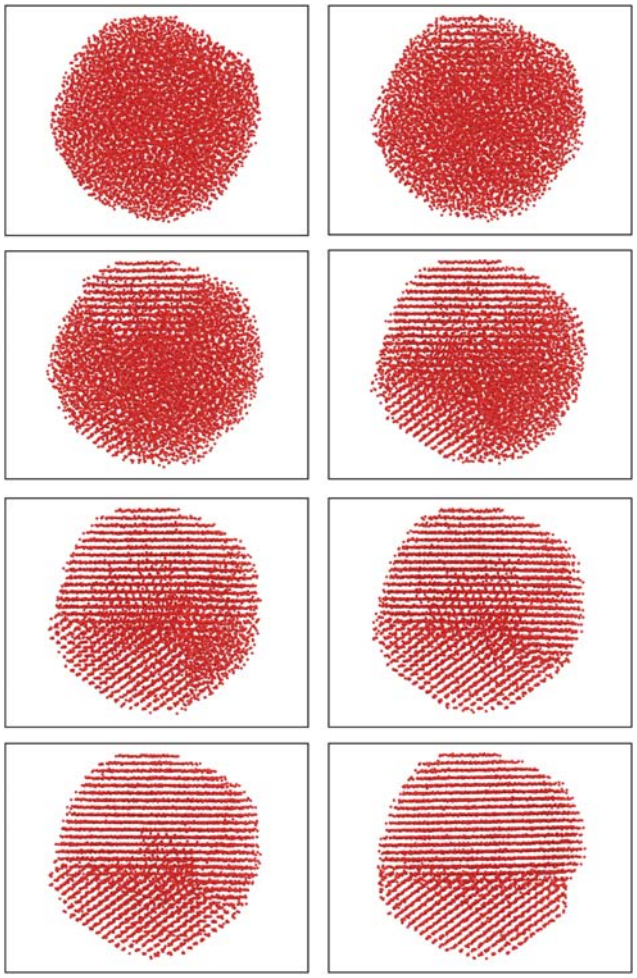

Fig. 3 Snapshots of the atom positions comprising the Li_2O nanoparticle (A), taken during the molecular dynamics simulation, revealing the evolution of a crystalline nanoparticle from an amorphous precursor; only the oxygen ions (red) are shown to improve clarity.

spontaneously evolved on the surface, Fig. 2. Specifically, the seed exposed {111} at the surface; previous *ab inito* simulations on Li_2O predicted that the (111) is the most stable surface.[36] The crystalline seed then nucleated the crystallisation of the surrounding (amorphous) Li and O ions. As the nanoparticle crystallises, the energy released is extracted by the thermostat to prevent re-amorphisation. However, before crystallisation was complete a second crystalline seed evolved within another amorphous region of the nanoparticle and resulted in the evolution of a grain-boundary as the crystallising fronts, emanating from the two (missoriented) seeds, impinged upon one another. Snapshots, taken during crystallisation, Fig. 3, reveal the evolution of the grain-boundary. The energy difference between the starting (amorphous) configuration and the final (crystalline) configuration, Fig. 1(a), reflects loosely the heat of crystallization.

The configurational energy plateaus a second time, with a slight negative gradient, which indicates a gradual increase in stability as the ions rearrange to facilitate a more energetically stable configuration. The configurational energy then drops sharply a second time, after about 1.8 ns, Fig. 1(a). Analysis of the structure revealed that this energy drop corresponds to the annealing out of the grain-boundary to form a monocrystal.

Inspection of the calculated RDF, Fig. 1(d), reveals that after 130 ps (red trace), the peaks are broad and poorly defined—indicative of an amorphous configuration. However, as the simulation continues, the peaks become sharper indicating an increase in the crystallinity of the nanoparticle. The RDF corresponding to the final, low (1 K) temperature, structure (black trace) is associated with the sharpest peaks. However, the nearest neighbour Li–O peak (black trace) reveals a 0.6 Å difference between the shortest and longest Li–O distance in the nanoparticle, which reflects the considerable relaxation of ions comprising the nanoparticle—especially those at low coordinated positions on the surface of the nanoparticle. We note that the crystallisation of system (C) also evolved multiple missoriented grains, Fig. 4, whereas system (B) remained a monocrystal throughout the crystallisation.

The final, low temperature structure of system (A) is shown in Fig. 5, and reveals that the nanocrystal conforms to the inverse fluorite structure and comprises an octahedral morphology with {111} truncated by {100}—similar to ceria nanoparticles.[27] This figure also shows a slice cut through the system showing the grain-boundaries before it had annealed out. Graphical techniques were used to ascertain that the interfacial plane of the grain-boundary exhibited two-dimensional curvature. It can perhaps be argued that the edges of the nanoparticle comprise {110}, Fig. 5, although these appear somewhat facetted. The low (1 K) temperature structures of all three nanoparticles, A, B and C, are shown in Fig. 6, the stability of which decrease in the order (A) > (B) > (C), where (A) is energetically the most stable configuration.

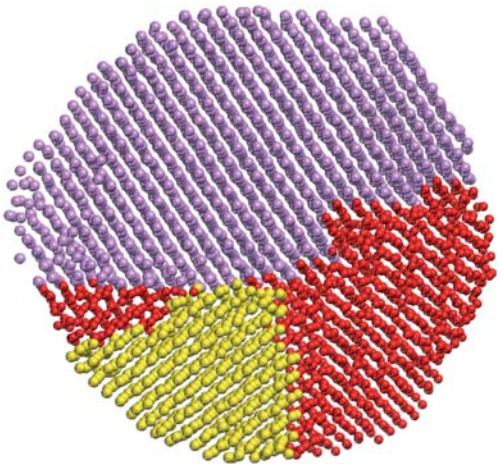

Fig. 4 Sphere model representation of the atom positions within a slice cut through the Li_2O nanoparticle (C) revealing the missoriented grains and grain-boundaries present within the nanoparticle. Only oxygen ions are shown with colour notation to highlight the individual grains.

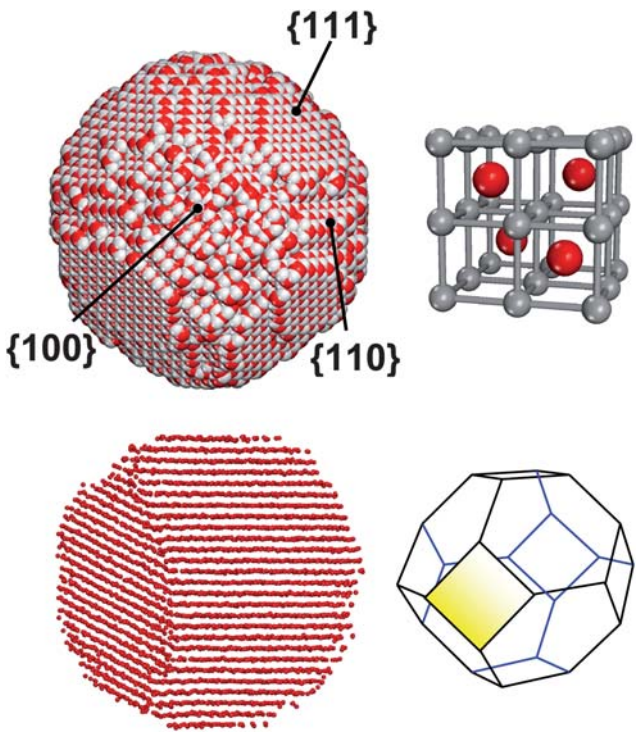

Fig. 5 Final, low temperature, structure of the Li_2O nanocrystal (A) top left. Top right shows a segment cut from this nanocrystal revealing the inverse fluorite structure; bottom left shows a slice cut through the nanocrystal revealing the grain-boundary before it had annealed out of the structure during prolonged MD; bottom right a schematic illustrating the truncated octahedral morphology. Lithium is coloured grey and oxygen is red.

The energy calculated as a function of time for nanoparticles (B) and (C), shown in Fig. 1(b and c), reveals that the speed of crystallisation is critically dependent upon the simulation conditions. Specifically, nanoparticle (C), which was crystallised at 700 K, required about 2 ns to crystallise, which compares with 0.5 ns and 0.27 ns for nanoparticles (A) and (B) respectively. We also note that (B) crystallises into a single crystal, whereas (C) comprises multiple grains—one of which anneals out after about 4–5 ns.

A previous simulation study using density functional theory by Seriani predicted an octahedral morphology for Li_2O nanoparticles.[37] In particular, the (111) surface was predicted to be much more stable compared to the (110) and especially the (100). However, these simulations considered the most thermodynamically stable morphology. Conversely, experiment has shown that kinetic aspects can play a pivotal role. In particular, similar to the models presented in this present study truncated octahedral nanoparticles of ceria have been observed.[27]

We note that inverse fluorite {100} surfaces are dipolar[38] and therefore a mechanism for quenching the dipole and thus stabilising the surface is needed. In many atomistic simulations, this is typically achieved by removing half the ions from the top layer and replacing them at the bottom to facilitate a neutral repeat. Specifically, in the case of Li_2O, with anti-fluorite structure, half the Li ions would need to be removed from the top—{100}—atomic layer and replaced at the bottom—{$\bar{1}$00}: atomic layer thus changing the stoichiometry from Li_2O to LiO for both {100} and {$\bar{1}$00}. Further details pertaining to this procedure can be found in ref. 38. Simulated crystallisation does not require (or indeed allow) the simulator to 'physically' move ions; rather the dipole is necessarily quenched during crystallisation and is driven in response to minimising the configuration energy. To determine how this was achieved, the trajectories of the ions during crystallisation were examined using graphical techniques and revealed, as one might expect, that the Li ions did not migrate the whole diameter of the nanoparticle, rather a concerted movement of ions (between {100} and {$\bar{1}$00}) within the surface layers was observed to facilitate the change in surface stoichiometry required to quench the dipole. We note that previous atomistic models of CeO_2 have proposed such a mechanism with experimental corroboration.[27]

The structure of the top atomic layer (100) is shown in Fig. 7(a), revealing LiO stoichiometry; the penultimate atomic layer, with Li_2O stoichiometry, is shown in Fig. 7(b). We note that at the perimeter of the penultimate layer, the stoichiometry is LiO because there are no layers above and the LiO exists at the surface as –Li–O–Li–O– chains. The nearest neighbour (oxygen) coordination number of Li ions range from two for Li located at {100} surfaces, edges and steps; three for Li on {111} surfaces and four for Li in the bulk of the nanoparticle.

A final consideration was the evolution of (point) defects. Analysis of the Li_2O nanoparticle (A) revealed a variety of point defects both on the surface and within the bulk of the nanocrystal. These include isolated O^{2-} and Li^+ vacancies, together with charged, for example $[V_{Li}V_O^{\bullet\bullet}]^{\bullet}$, and charge neutral, $[2V_{Li}V_O^{\bullet\bullet}]^x$, vacancy clusters. The structures of two such defect clusters are shown in Fig. 7(c and d). We note that the number of atoms and hence stoichiometry of the nanoparticle remains fixed and charge neutral during the simulation.

We also explored ionic mobility within the model nanostructure. In particular, the structure of particle C, after 9 ns of MD simulation, is shown in Fig. 7(e); five atomic layers in the middle of the nanoparticle are enlarged to help one visualise the ionic mobility. After a further 10 ns, Fig. 7(f and g), one can see

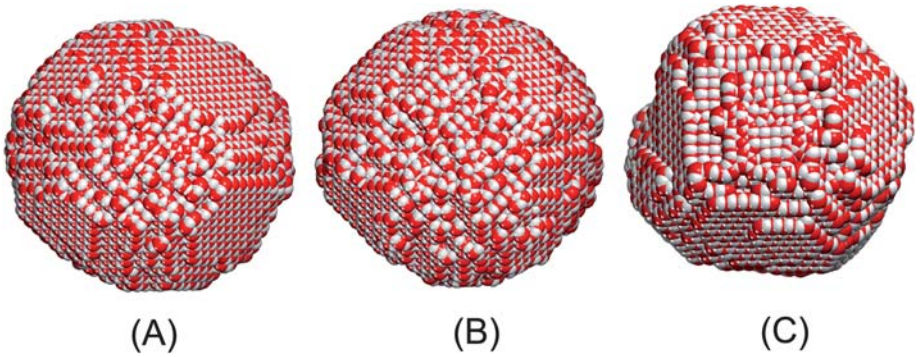

Fig. 6 Atomistic structures of the three Li_2O nanoparticles (A), (B) and (C). Lithium is coloured grey and oxygen is red.

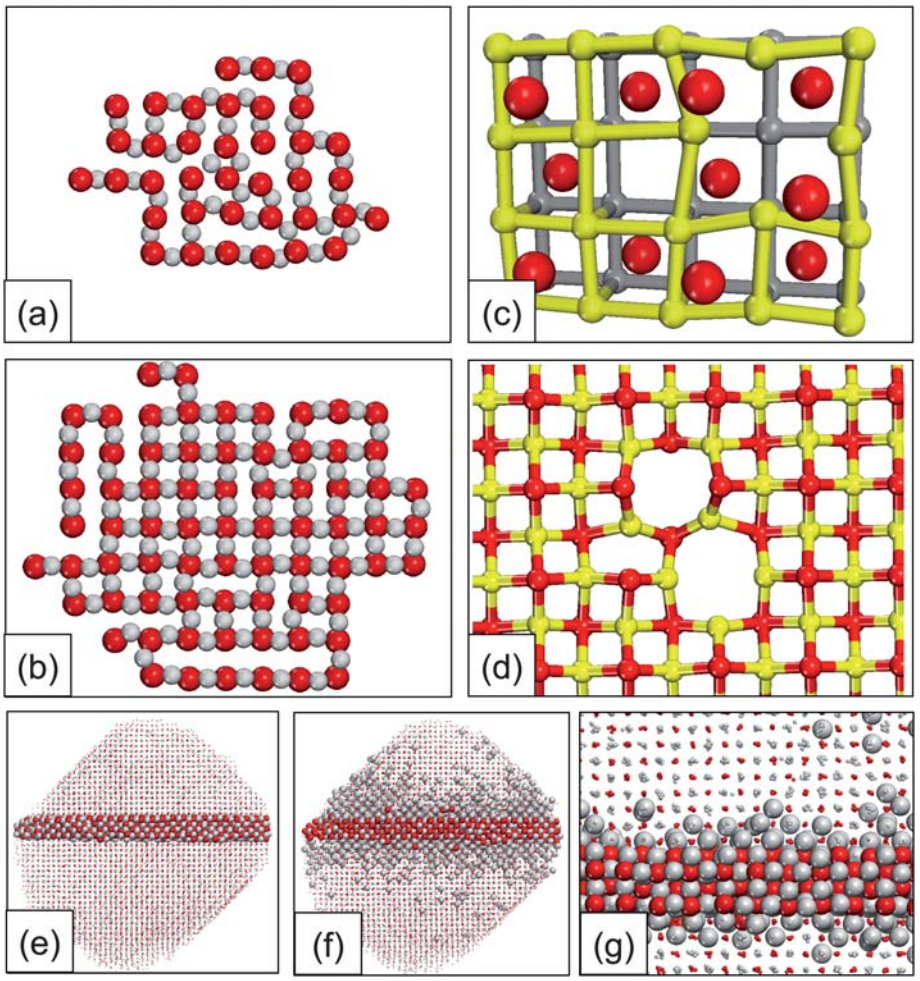

Fig. 7 Structure of the surface atomic layer (a) and penultimate surface atomic layer (b) of the (dipolar) (100) surface revealing how the dipole is quenched *via* a 50% reduction of Li ions at the surface to give LiO stoichiometry; (c) and (d) reveal the structure of point defects that have evolved within the Li_2O nanocrystals; (e) Li_2O nanocrystal (C) after 9 ns of MD and (f) after 19 ns of MD simulation revealing the mobility of the Li ions; (g) enlarged segment of (f). Oxygen is coloured red and Li is grey or yellow.

that there is significant mobility of Li^+ ions; O^{2-} ions remain at their start position. The mobility is highest around the surface of the nanoparticle, but Li ions are also observed to have moved within the 'bulk' regions of the nanoparticle. Close inspection of the behaviour using graphical techniques reveals that the Li ion mobility is (Li) vacancy driven within the bulk region of the nanoparticle. Strange and co-workers used ^{7}Li NMR relaxation time and A.C. conductivity measurements to explore ionic transport in Li_2O and established that the mobile ions are Li^+ and that diffusion is (cation) vacancy driven,[39] in accord with our simulation. Such experimental corroboration helps validate our result albeit our simulations consider a Li_2O nanoparticle. The

same study acknowledges that O ion mobility is very small. Cation and anion vacancy formation energies together with ionic transport have been calculated in Li_2O previously by Gavartin and co-workers;[9] superionic behaviour in Li_2O has also been reported previously.[40]

Discussion

Our results show that changes to the simulation conditions, in this case temperature, facilitate the generation of atomistic models with diverse microstructures. For example, the simulation conditions exact a critical influence over the crystallisation and led to nanoparticles (A) and (C) evolving multiple grains, yet (B) remained a monocrystal. However, robust conclusions, pertaining to the influence of the simulation conditions with respect to microstructure, such as 'lower temperatures favour the evolution of multiple grains', cannot yet be drawn from these results; rather statistically viable nanostructure distributions are needed.

The simulations performed in this present study best reflect experimental synthesis of nanoparticles *via* melting and crystallisation.[27] In particular, we have shown that by simulating, in part, experimental conditions, one can capture important‡ structural features observed experimentally. This includes structural distributions of morphology, defect concentrations and grain boundaries. And while such features can be introduced using more traditional simulation approaches, certain structures, such as grain-boundaries with two-dimensionally curved interfacial planes, structural modifications to facilitate quenching of dipolar surfaces, defect distributions and defect types influenced by the simulation conditions, may be more easily generated using such 'evolutionary' simulation strategies. In addition, synergistic interactions between microstructural features, which may result in structural modification, will also be captured within a (single) atomistic model as the material evolves structurally during crystallisation. On the other hand, structural changes that can occur over long experimental timescales, for example creep, are not currently accessible using the approach presented in this present study. Nevertheless simulation strategies to overcome these issues are being developed, for example strategies for simulating creep can be found in ref. 41. In addition, constructing structures, informed by experiment, 'by-hand', which have been used since the inception of atomistic simulation, can still provide unique and invaluable methods of control. We propose that the methods detailed in this study are complementary to alternative simulation methodologies and combined simulation strategies will further enhance the 'truly predictive' capability of atomistic simulation. In particular, atomistic simulation coupled with finite element analysis or computational fluid dynamics on one side[42] and *ab initio* approaches, such as density functional theory[43] on the other, together with methods for accelerated dynamics, have enabled simulation to span considerable length and timescales.

Conclusion

Atomistic computer simulation can be used to predict the properties of a material to inform experiment. However, many material properties are governed by its microstructure and therefore if one is to simulate properties reliably, then such microstructural features must be captured within the atomistic model. In many cases, microstructure evolves within a real material during synthesis. Here, we have attempted to capture, in part, key aspects pertaining to synthesis to evolve the atomistic model. Specifically, we use simulated crystallisation to generate atomistic models for Li_2O nanoparticles starting from amorphous precursors. Moreover, by changing the simulation conditions, we were able to exact changes upon the microstructures of the nanoparticle. In particular, changes in the simulation temperature resulted in subtle morphological differences such as steps edges, and also more significant microstructural differences, including grain-boundaries.

The resulting atomistic models of Li_2O were predicted to comprise polyhedral morphologies with {100} truncated {111} together with {110} edges and conforming to the inverse fluorite crystal structure. The models also incorporate microstructural features including grain-boundaries and isolated and associated Li, O vacancies; mobile ions were calculated to be Li^+ and the diffusion mechanism (Li) vacancy driven. Dipolar {100} surfaces were quenched *via* a change in the stoichiometry of the surface atomic layers from Li_2O to LiO, which occurs during crystallisation and is energetically driven.

Accordingly, atomistic simulation can be used to generate models that capture the (micro)structural diversity and structural distributions observed experimentally.

‡ In that they influence the properties of the material.

Acknowledgements

South African Research Chair Initiative of the Department of Science and Technology; National Research Foundation and the Centre for High performance Computing (CHCP) in South Africa.

References

1 E. A. Davis, *J. Phys.: Condens. Matter*, 2007, **19**, 251001.
2 V. Yamakov, D. Wolf, S. R. Phillpot, A. K. Mukharjee and H. Gleiter, *Nat. Mater.*, 2004, **3**, 43–47.
3 S. C. Tjong and H. Chen, *Nanocrystalline Materials and Coatings*, *Mat. Sci. Eng. R*, 2004, 45, 1–88.
4 X. W. Liu, K. B. Zhou, L. Wang, B. Y. Wang and Y. D. Li, *J. Am. Chem. Soc.*, 2009, **131**, 3140–3141.
5 A. Taguchi and F. Schuth, *Microporous Mesoporous Mater.*, 2005, **77**, 1–45.
6 J. D. Gale, *Z. Kristallogr.*, 2005, **220**, 552–554.
7 J. P. Allen, W. Gren, M. Molinari, C. Arrouvel, F. Maglia and S. C. Parker, *Mol. Simul.*, 2009, **35**, 584–608.
8 C. A. J. Fisher and H. Matsubara, *Philos. Mag.*, 2005, **85**, 1067–1088.
9 J. L. Gavartin, C. R. A. Catlow, A. L. Shlugertt, A. N. Varaksin and Y. N. Kolmogorovs, *Modell. Simul. Mater. Sci. Eng.*, 1992, **1**, 29–38.
10 A. M. Walker, B. Slater, J. D. Gale and K. Wright, *Nat. Mater.*, 2004, **3**, 715–720.
11 G. W. Watson, E. T. Kelsey, N. H. de Leeuw, D. J. Harris and S. C. Parker, *J. Chem. Soc., Faraday Trans.*, 1996, **92**, 433–438.
12 D. M. Duffy, *J. Phys. C: Solid State Phys.*, 1986, **19**, 4393–4412.
13 T. X. T. Sayle, C. R. A. Catlow, D. C. Sayle and S. C. Parker, *Philos. Mag. A*, 1993, **68**, 565–573.
14 C. A. J. Fisher, V. M. H. Prieto and M. S. Islam, *Chem. Mater.*, 2008, **20**, 5907–5915.
15 J. Schiotz, T. Di, F. D. Tolla and K. W. Jacobson, *Nature*, 1998, **391**, 561–561.
16 Q. Yuan, H. Duan, L. Li, L. Sun, Y. Zhang and C. Yan, *J. Colloid Interface Sci.*, 2009, **335**, 151–167.

17 G. Mobus and B. J. Inkson, *Mater. Today*, 2007, **10**, 18–25.
18 S. Piana, M. Reyhani and J. D. Gale, *Nature*, 2005, **438**, 70–73.
19 D. C. Sayle, S. A. Maicaneanu, B. Slater and C. R. A. Catlow, *J. Mater. Chem.*, 1999, **9**, 2779–2787.
20 D. W. Lewis, D. J. Willock, C. R. A. Catlow, J. M. Thomas and G. J. Hutchings, *Nature*, 1996, **382**, 604–606.
21 X. M. Bai, A. F. Voter, R. G. Hoagland, M. Nastasi and B. P. Uberuaga, *Science*, 2010, **327**, 1631–1634.
22 B. Coasne, A. Mezy, R. J. M. Pellenq, D. Ravot and J. C. Tedenac, *J. Am. Chem. Soc.*, 2009, **131**, 2185–2198.
23 N. S. Froemming and G. Henkelman, *J. Chem. Phys.*, 2009, **131**, 234103.
24 N. Castin and L. Malerba, *J. Chem. Phys.*, 2010, **132**, 074507.
25 P. Jajarmi and S. Valipour, *Comput. Mater. Sci.*, 2009, **47**, 384–387.
26 D. C. Sayle and T. X. T. Sayle, *J. Comput. Theor. Nanosci.*, 2007, **4**, 299–308.
27 X. D. Feng, D. C. Sayle, Z. L. Wang, M. S. Paras, B. Santora, A. C. Sutorik, T. X. T. Sayle, Y. Yang, Y. Ding, X. D. Wang and Y. S. Her, *Science*, 2006, **312**, 1504–1508.
28 P. G. Bruce, B. Scrosati and J. M. Tarascon, *Angew. Chem., Int. Ed.*, 2008, **47**, 2930.
29 M. Armand and J. M. Tarascon, *Nature*, 2008, **451**, 652.
30 P. Goel, N. Choudhury and S. L. Chaplot, *Trans. Indian Inst. Met.*, 2009, **62**, 141–147.
31 P. Goel, N. Choudhury and S. L. Chaplot, *J. Phys.: Condens. Matter*, 2007, **19**, 386239.
32 F. Jiao and P. G. Bruce, *Adv. Mater.*, 2007, **19**, 657–660.
33 T. X. T. Sayle, S. C. Parker and D. C. Sayle, *Faraday Discuss.*, 2007, **134**, 377–397.
34 T. X. T. Sayle, P. E. Ngoepe and D. C. Sayle, *ACS Nano*, 2009, **3**, 3308–3314.
35 W. Smith and T. R. Forester, DL_POLY, copyright by the council for the Central Laboratory of the Research Councils, Daresbury Laboratory, Daresbury, Warrington, UK, 1996, www.cse.clrc.ac.uk/msi/software/DL_POLY/.
36 M. M. Islam and T. Bredow, *J. Phys. Chem. C*, 2009, **113**, 672–676.
37 N. Seriani, *Nanotechnology*, 2009, **20**, 445703.
38 J. H. Harding, *Surf. Sci.*, 1999, **422**, 87.
39 J. H. Strange, S. M. Rageb, A. V. Chadwick, K. W. Flack and J. H. Harding, *J. Chem. Soc., Faraday Trans.*, 1990, **86**, 1239–1241.
40 R. M. Fracchia, G. D. Barrera, N. L. Allan, T. H. K. Barron and W. C. Mackrodt, *J. Phys. Chem. Solids*, 1998, **59**, 435–445.
41 T. T. Lau, A. Kushima and S. Yip, *Phys. Rev. Lett.*, 2010, **104**, 175501.
42 K. Kalweit and D. Drikakis, *J. Comput. Theor. Nanosci.*, 2008, **5**, 1923–1938.
43 P. Sherwood, et al., *J. Mol. Struct. (Theochem)*, 2003, **632**, 1–28.

